Nanoscale

RSC Publishing

PAPER

View Article Online
View Journal | View Issue

Cite this: *Nanoscale*, 2013, **5**, 2442

Facile synthesis of loaf-like $ZnMn_2O_4$ nanorods and their excellent performance in Li-ion batteries†

Zhongchao Bai,*[a] Na Fan,[b] Changhui Sun,[b] Zhicheng Ju,[b] Chunli Guo,[a] Jian Yang*[c] and Yitai Qian[bc]

Binary transition metal oxides have been attracting extensive attention as promising anode materials for lithium-ion batteries, due to their high theoretical specific capacity, superior rate performance and good cycling stability. Here, loaf-like $ZnMn_2O_4$ nanorods with diameters of 80–150 nm and lengths of several micrometers are successfully synthesized by annealing MnOOH nanorods and $Zn(OH)_2$ powders at 700 °C for 2 h. The electrochemical properties of the loaf-like $ZnMn_2O_4$ nanorods as an anode material are investigated in terms of their reversible capacity, and cycling performance for lithium ion batteries. The loaf-like $ZnMn_2O_4$ nanorods exhibit a reversible capacity of 517 mA h g^{-1} at a current density of 500 mA g^{-1} after 100 cycles. The reversible capacity of the nanorods still could be kept at 457 mA h g^{-1} even at 1000 mA g^{-1}. The improved electrochemical performance can be ascribed to the one-dimensional shape and the porous structure of the loaf-like $ZnMn_2O_4$ nanorods, which offers the electrode convenient electron transport pathways and sufficient void spaces to tolerate the volume change during the Li^+ intercalation. These results suggest the promising potential of the loaf-like $ZnMn_2O_4$ nanorods in lithium-ion batteries.

Received 17th October 2012
Accepted 4th January 2013

DOI: 10.1039/c3nr33211j

www.rsc.org/nanoscale

Introduction

Rechargeable lithium-ion batteries (LIBs), as one of the most important devices for energy storage and conversion, have attracted tremendous attention in the past decades.[1–4] They have gained great successes in small mobile electronics, such as MP3 players, cellular phones, digital cameras, portable computers, and so on. But almost all the anode materials for commercial LIBs are based on graphite that only has a theoretical specific capacity of 372 mA h g^{-1}. Such a small capacity cannot meet the demand of high-energy applications like electric vehicles.[5] Thus, other anode materials with a high capacity are urgently demanded. Transition metal oxides (*e.g.*, Co_3O_4, Fe_2O_3, Mn_3O_4 and $ZnMn_2O_4$) have been considered as promising anode materials owing to their high theoretical specific capacity.[6–9] However, their applications in LIBs are hindered by the poor cycling performance due to a significant volume change during Li insertion/extraction.[10,11] In addition, an inferior rate performance is another limitation for their applications in LIBs. Recently, reduction of these materials to the nanoscale is an effective method to address the above issues.[12–15] One-dimensional nanomaterials are particularly attractive, owing to their large surface-to-volume ratio that allows for efficient electrode–electrolyte contact and excellent one-dimensional electron transport pathways.[16–18] Meanwhile, porous structures could preserve the electrode integrity and then improve the structure stability of the electrode, due to their good tolerance to the volume variation during discharge–charge processes.[19–22] Thus, if the porous structure can be introduced into one-dimensional nanomaterials, the resulting porous nanorods will combine the advantages of porous nanostructure and one-dimensional geometry. Such a structure is most likely to have an excellent performance in LIBs.

Among the transition metal oxides, $ZnMn_2O_4$ has many advantages, such as environmental friendliness, low cost, and much lower operating voltage in comparison with the Co or Fe-based oxides.[23–25] The anode material with a lower charge voltage can deliver a higher energy density. Therefore, $ZnMn_2O_4$ has been considered as a promising anode candidate to replace commercial graphite for LIBs. To date, $ZnMn_2O_4$ nanomaterials in different morphologies, such as nanoparticles, nanowires, nanoflowers and nanoflakes, have been explored for LIBs.[23–29] Deng and Chen synthesized the agglomerated $ZnMn_2O_4$ nanoparticles by the calcination of a Zn–Mn citrate complex.[23] The nanoparticles showed an average specific capacity of 555 mA h g^{-1} at 200 mA g^{-1} or 405 mA h g^{-1} at 600 mA g^{-1}. Kim and Kang

[a]*Research Institute of Surface Engineering, Taiyuan University of Technology, Taiyuan, 030024, China. E-mail: baizhongchao@tyut.edu.cn; Tel: +86 351 6010540*

[b]*Hefei National Laboratory for Physical Science at Microscale and Department of Chemistry, University of Science and Technology of China, Hefei, 230026, China*

[c]*School of Chemistry and Chemical Engineering, Shandong University, Jinan 250100, China. E-mail: yangjian@sdu.edu.cn*

† Electronic supplementary information (ESI) available: Nitrogen adsorption–desorption isotherms; XRD pattern of $ZnMn_2O_4$ synthesized at 600 °C; the TEM images of the $ZnMn_2O_4$ nanorods prepared at 800 °C for 2 h; SEM images of $ZnMn_2O_4$ obtained at 700 °C for 10 h. See DOI: 10.1039/c3nr33211j

reported a solid-state reaction of $Zn(Ac)_2$ and α-MnO_2 nanowires at a high temperature for $ZnMn_2O_4$ nanowires.[25] The nanowires presented the reversible capacities of 450 mA h g^{-1} at 500 mA g^{-1} or 350 mA h g^{-1} at 1000 mA g^{-1} after 40 cycles. To the best of our knowledge, the preparation of the porous $ZnMn_2O_4$ nanorods has not been reported before, due to its distinct spinel structure.

In this work, we report a facile method for the synthesis of loaf-like $ZnMn_2O_4$ nanorods by annealing MnOOH nanorods and $Zn(OH)_2$ at 700 °C for 2 h. The crystal structure and morphology of the loaf-like $ZnMn_2O_4$ nanorods are characterized by XRD, SEM, TEM, and FT-IR techniques. Cyclic voltammograms (CV) and galvanostatic discharge–charge cycling indicate that the loaf-like $ZnMn_2O_4$ nanorods are a superior anode material for LIBs. At a current density of 500 mA g^{-1}, the nanorods still maintain a reversible capacity of 517 mA h g^{-1} after 100 cycles. Even at 1000 mA g^{-1}, the reversible capacity of the nanorods is kept at 457 mA h g^{-1}.

Experimental section

Synthesis of MnOOH and $ZnMn_2O_4$ nanorods

Synthesis of MnOOH nanorods. In a typical procedure,[30,31] 0.2 g of $KMnO_4$ and 5 mL of PEG 400 were added into 40 mL of distilled water and vigorously stirred at room temperature, producing a dark brown solution. This solution was poured into a Teflon-lined autoclave with a capacity about 60 mL. After the autoclave was heated at 160 °C for 3 h, then the solution was filtered and the as-obtained product was washed with distilled water and absolute ethanol several times. Finally, the product was collected and dried at 60 °C for 12 h in air.

Synthesis of loaf-like $ZnMn_2O_4$ nanorods. 0.286 g of $Zn(OH)_2$ powder and 0.493 g of the as-prepared MnOOH nanorods were dispersed in 5 mL of acetone. The solution was ball-milled for 5 h in order to generate a slurry. The slurry was then dried at 70 °C in air. Afterwards, the well-mixed mixture was calcined at 700 °C for 2 h in air. The brown powder was collected for the LIBs tests.

Electrochemical measurements

The electrodes for electrochemical properties were prepared with 60 wt% active material of $ZnMn_2O_4$, 30 wt% conducting acetylene black, and 10 wt% polyvinylidene fluoride (PVDF) binder in *N*-methyl-2-pyrrolidone (NMP). This mixture was pasted on a clean copper foil and then dried in vacuum at 80 °C for 12 h. The coated foil was then roll-pressed and cut into a disc. The cell was fabricated by using lithium foil as the counter electrode and the reference electrode, Celgard 2400 as the separator, and a solution of 1 M $LiPF_6$ in a mixture of ethylene carbonate (EC) and dimethyl carbonate (DMC) (1 : 1 v/v) as the electrolyte. The assembly of the cell was carried out in an argon-filled glove-box. The cell was discharged and charged from 0.01 to 3.0 V at different rates (Land CT2001A). Cyclic voltammograms (CV) were performed on a CHI-760 electrochemical workstation over the potential range of 0.01–3.0 V at a scan rate of 0.1 mV s^{-1}.

Structural characterization

The phases of the products were characterized by X-ray powder diffraction (XRD) technique using a Bruker D8 advanced X-ray diffractometer equipped with graphite-monochromatized Cu Kα radiation (Kα = 1.5418 Å). Fourier transform infrared (FT-IR) spectra were measured on a Shimadzu FTIR-8400S spectrometer. The scanning electron microscope images were taken with a JEOL JSM-7600F field-emission scanning electron microscope. The high-resolution transmission electron microscope (HRTEM) images were recorded on a JEOL-2100 high-resolution transmission electron microscope at an acceleration voltage of 200 kV. Nitrogen sorption isotherm was performed on a Tristar II 3020M gas sorptometer.

Results and discussion

XRD patterns of the as-prepared MnOOH nanorods and loaf-like $ZnMn_2O_4$ nanorods are shown in Fig. 1. All the diffraction peaks in Fig. 1a and b could be attributed to monoclinic MnOOH (JCPDS card no. 41-1379) and the tetragonal $ZnMn_2O_4$ (JCPDS card no. 24-1133), respectively.[24] The strong and narrow diffraction peaks indicate the good crystallinity of the as-prepared $ZnMn_2O_4$. The FTIR spectrum of the loaf-like $ZnMn_2O_4$ nanorods is shown in Fig. 2. The peak at 452 cm^{-1} can be ascribed to Zn–O stretching.[32] The peaks at 505, 627 and 669 cm^{-1} arise from Mn–O.[33] The results further confirm the formation of $ZnMn_2O_4$.

Transmission electron microscopy (TEM) and scanning electron microscopy (SEM) are used to reveal the morphology and microstructure of the as-prepared MnOOH and $ZnMn_2O_4$ nanorods. Fig. 3a and b show that MnOOH consists of nanorods with diameters of 80–150 nm and lengths of several micrometers. The smooth surface and uniform contrast throughout the nanorods indicate the absence of the pores inside the nanorods. Fig. 3c shows a representative HRTEM image of a single nanorod of MnOOH. The interplanar spacing is about 0.24 nm corresponding to the {002} plane of MnOOH. The obtained $ZnMn_2O_4$ maintains the one-dimensional shape of the MnOOH nanorods. Most importantly, although the magnified SEM images show a smooth surface for the $ZnMn_2O_4$ nanorod (Fig. 3d), a pore-like structure is observed throughout the whole nanorod (Fig. 3e). So, it can be concluded

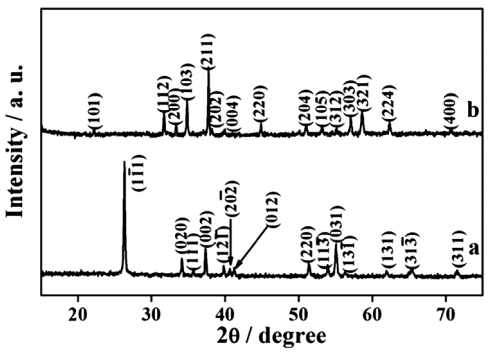

Fig. 1 The XRD patterns of (a) MnOOH and (b) $ZnMn_2O_4$.

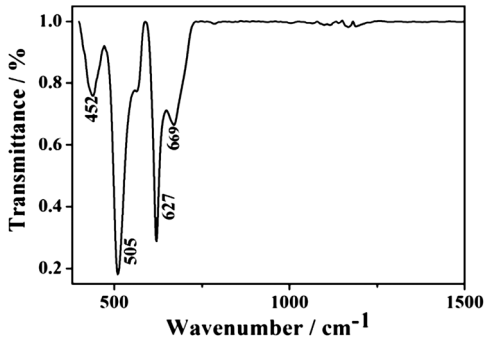

Fig. 2 The FT-IR spectrum of the as-prepared $ZnMn_2O_4$.

that the $ZnMn_2O_4$ nanorods have pore structures inside their bodies just like loafs that also present a relative smooth surface and have pores in their bodies (Fig. 3g). As shown in the inset of Fig. 3d, the hollow interior inside a broken $ZnMn_2O_4$ nanorod can be clearly identified. The porous feature of the $ZnMn_2O_4$ nanorods is also confirmed by BET measurements (ESI, Fig. S1†). The obvious hysteresis loop indicates the presence of tiny pores in the product. Because the $ZnMn_2O_4$ nanorods are prepared *via* a solid-state reaction, the as-produced pores are less controlled, resulting in a multi-model pore size distribution.

A typical HRTEM image of a single loaf-like $ZnMn_2O_4$ nanorod is shown in Fig. 3f. The interplanar distance is 0.25 nm, which is in good agreement with the (211) plane of tetragonal $ZnMn_2O_4$. This result also suggests the growth direction of the $ZnMn_2O_4$ nanorods is along the direction of [211].

The reaction time and temperatures are crucial for the synthesis of loaf-like $ZnMn_2O_4$ nanorods. When the reaction temperature is lower than 600 °C, $ZnMn_2O_4$ nanorods with a poor crystallinity are obtained (ESI, Fig. S2†). Increasing the reaction temperature to 800 °C results in $ZnMn_2O_4$ nanorods without porous structures (ESI, Fig. S3a†). This phenomenon is very common in the solid state reactions.[34,35] Reducing the reaction time cannot guarantee that the raw materials react completely. Increasing the reaction time would destroy the loaf-like structures and produce many micro-particles (ESI, Fig. S3b†). Therefore, we believe that the optimal temperature and reaction time for loaf-like $ZnMn_2O_4$ nanorods are 700 °C and 2 h, respectively. The formation mechanism of the porous structures in the nanorods is probably related to the decomposition of the hydroxides and/or the reaction between ZnO and MnO_2.[36,37]

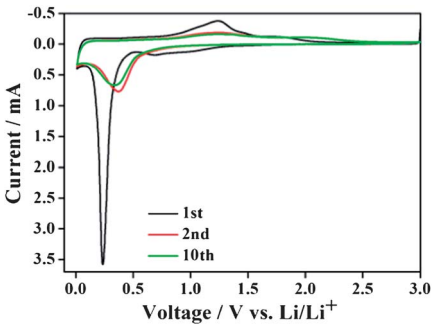

Fig. 4 Cyclic voltammograms of the loaf-like $ZnMn_2O_4$ nanorods in the voltage range of 0.01–3.0 V at a scan rate 0.1 mV s^{-1}.

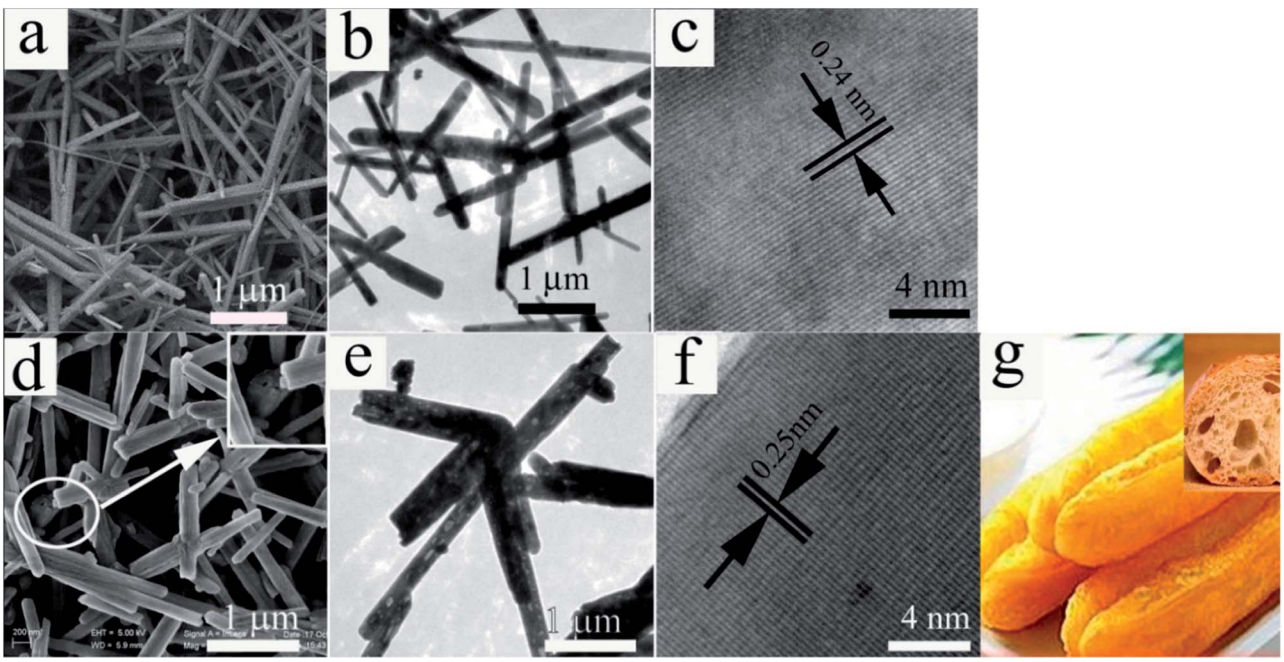

Fig. 3 (a) SEM, (b) TEM, and (c) HRTEM images of the MnOOH nanorods, (d) SEM, (e) TEM and (f) HRTEM images of the loaf-like $ZnMn_2O_4$ nanorods. (g) A real-color image of a loaf to illustrate the morphology of the $ZnMn_2O_4$ nanorods.

The electrochemical activity of the loaf-like $ZnMn_2O_4$ nanorods as an anode material for LIBs is examined by cyclic voltammograms (CV) and galvanostatic cycling. Fig. 4 represents the CV curves of $ZnMn_2O_4$ electrode carried out at a scan rate of 0.1 mV s^{-1} in the voltage range of 0.01–3.0 V *versus* Li/Li^+. During the first cathodic scan, three peaks are observed at around 1.1, 0.7 and 0.25 V, respectively. The reduction peak at 1.1 V disappears in the subsequent scans, corresponding to the reduction of Mn^{3+} to Mn^{2+}.[38] The reduction peak at 0.7 V might be attributed to the irreversible decomposition of the electrolyte and the formation of the solid electrolyte interphase (SEI) as reported in graphite electrodes.[38] This peak also fades away in the following scans. The intensive peak at 0.25 V could be attributed to the reduction of $ZnMn_2O_4$ to Zn^0 and Mn^0 embedded in Li_2O matrix, and the formation of the Li–Zn alloy.[37,39] During the subsequent anodic sweep, the two oxidation peaks can be ascribed to the decomposition of the Li_2O matrix and the formation of MnO at 1.20 V and ZnO at 1.5 V, respectively.[26,27] In the following scans, the reduction peak moves to 0.5 V, which could be associated with the reduction of MnO and ZnO to Mn^0 and Zn^0, and the formation of Zn–Li alloy. While the oxidation peaks are analogous to the first scan, suggesting the similar electrochemical processes for the anodic scans.

The first and second discharge–charge curves of the loaf-like $ZnMn_2O_4$ nanorods for Li-ion batteries are shown in Fig. 5a, which are recorded at 100 mA g^{-1} at room temperature in the voltage range of 0.01 to 3.00 V (*versus* Li/Li^+). The as-prepared $ZnMn_2O_4$ shows two apparent voltage plateaus between 0.01 and 3.00 V in the first discharge process, delivering a total capacity of 1357 mA h g^{-1} higher than those of the reported $ZnMn_2O_4$ nanocrystals (1032 mA h g^{-1}) and nanoflakes (1088 mA h g^{-1}).[23,24] The first voltage plateau at 1.21 V corresponds to the reducing of Mn^{3+} to Mn^{2+}. The second voltage plateau at 0.43 V is related to the formation of Mn^0, Zn^0 and Li–Zn alloy. The first charge curve from 0.01 to 3.00 V shows a steady and smooth voltage increase (overall capacity of 839 mA h g^{-1}). So, there is an irreversible loss of 518 mA h g^{-1} between the first discharge and charge cycles. The initial coulombic efficiency is 61.8%, which is slightly higher than those of the $ZnMn_2O_4$ nanocrystals (58.8%) and nanoflowers (56.5%).[24,28] This result might be related to the small specific surface area of the porous nanorods, reducing the capacity from the irreversible reactions on the surface. In the second discharge cycle, the primary potential plateau moves to nearly 0.75 V (*versus* Li^+/Li). After the second cycle, the voltage profile does not change much compared with the second cycle. This result is in good agreement with the CV measurements.

Fig. 5b shows the plot of the charge–discharge capacity of loaf-like $ZnMn_2O_4$ nanorods *versus* cycle number. During the first several cycles, there is a relatively high capacity loss. The charge capacity loses about 20% of its initial capacity after the first 10 cycles. This phenomenon is also observed in other oxides, which is ascribed to the formation of a stable SEI layer on the electrode surface as well as the establishment of a compact electric contact with the current collector during the initial cycles.[24,40] Hereafter, the electrode displays an excellent cycling performance and the coulombic efficiency is higher than 98%. After the 50th cycle, there is a slight capacity increase until the 80th cycle.[21] Finally, the electrode preserves a specific capacity of 517 mA h g^{-1} after 100 cycles at a current density of 500 mA g^{-1}, much higher than the previous reports.[25,29,41] $ZnMn_2O_4$ nanowires prepared by a solid-state reaction of $Zn(Ac)_2$ and α-MnO_2 delivered a specific capacity of 450 mA h g^{-1} at the same current density after 40 cycles.[25] Porous $ZnMn_2O_4$ nanoplates synthesized from a metal–organic framework (MOF) precursor exhibited a 502 mA h g^{-1} at 60 mA g^{-1} after 30 cycles.[29] $ZnMn_2O_4$ nanoparticles with a diameter less than 5 nm only showed a specific capacity of 430 mA h g^{-1} at a rate of C/10 after 100 cycles.[41] The improved performance of the loaf-like nanorods is derived from its one-dimensional shape and the porous structure, providing efficient electron transport pathways, large surface-to-volume ratio, and effective tolerance to the volume change when lithium ions diffuse into/out the electrode.

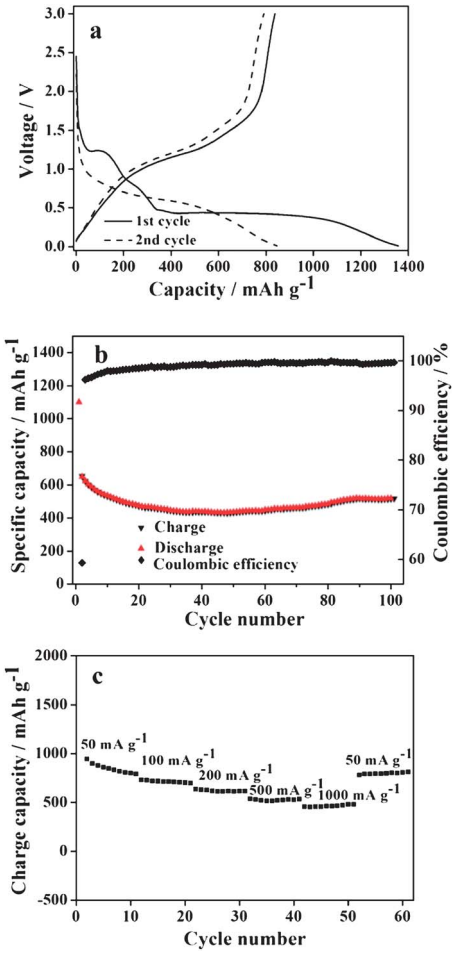

Fig. 5 (a) Discharge–charge profiles of the loaf-like $ZnMn_2O_4$ nanorods at 100 mA g^{-1} in the voltage range of 0.01–3.0 V. (b) Discharge–charge capacities *vs.* cycle number for the loaf-like $ZnMn_2O_4$ nanorods at a rate of 500 mA g^{-1}. (c) Cycling performance of the loaf-like $ZnMn_2O_4$/Li cell at different discharge current densities.

Besides the high specific capacity and good cyclability, the rate capability is also important for high performance LIBs. The rate capabilities of the prepared $ZnMn_2O_4$ material are presented in Fig. 5c. The charge capacities of 810, 712, 615, and 522 mA h g^{-1} are observed, as the current density increases from 50, to 100, 200, or 500 mA g^{-1} respectively. Even at a current density of 1000 mA g^{-1}, the specific capacity of the loaf-like $ZnMn_2O_4$ nanorods also remains at 457 mA h g^{-1}, which is higher than that of the $ZnMn_2O_4$ nanowires (350 mA h g^{-1}).[24] Additionally, the specific capacity is able to return to 810 mA h g^{-1} when the current density is again reduced to 50 mA g^{-1}. The above results indicate that the loaf-like $ZnMn_2O_4$ nanorods are a promising anode candidate for the LIBs.

Conclusions

The loaf-like $ZnMn_2O_4$ nanorods were successfully synthesized through a simple solid-state reaction of MnOOH nanorods and $Zn(OH)_2$ at 700 °C for 2 h. Both XRD pattern and TEM images confirm the formation of the loaf-like $ZnMn_2O_4$ nanorods. The effects of the reaction temperature and reaction time on the products are also investigated in detail. The loaf-like $ZnMn_2O_4$ nanorods show a reversible specific capacity of 517 mA h g^{-1} at a current densities of 500 mA g^{-1} after 100 cycles. Even at 1000 mA g^{-1}, the reversible capacity of the nanorods still could be kept at 457 mA h g^{-1}. The enhanced electrochemical performances of the loaf-like $ZnMn_2O_4$ nanorods can be attributed to their one-dimensional shape and the porous structure, which offer the electrode efficient electron transport pathways and sufficient void spaces to tolerate the volume change during the lithiation process.

Acknowledgements

This work was supported by the 973 Project of China (no. 2011CB935901), the National Nature Science Foundations of China (no. 91022033, 21071055, and 51172076), New Century Excellent Talents in University (NCET-10-0369), Shandong Provincial Natural Science Foundation for Distinguished Young Scholar (JQ201205), Independent Innovation Foundations of Shandong University (2012ZD007), and new-faculty start-up funding in Shandong University. We would like to thank Prof. Weiliu Fan for helpful discussion.

Notes and references

1 P. G. Bruce, B. Scrosati and J. M. Tarascon, *Angew. Chem., Int. Ed.*, 2008, **47**, 2930.
2 M. R. Palacın, *Chem. Soc. Rev.*, 2009, **38**, 2565.
3 P. Poizot and F. Dolhem, *Energy Environ. Sci.*, 2011, **4**, 2003.
4 O. K. Park, Y. Cho, S. Lee, H. C. Yoo, H. K. Song and J. Cho, *Energy Environ. Sci.*, 2011, **4**, 1621.
5 M. S. Whittingham, *Dalton Trans.*, 2008, 5424.
6 C. M. Doherty, R. A. Caruso and C. J. Drummond, *Energy Environ. Sci.*, 2010, **3**, 813.
7 J. Liu, T. E. Conry, X. Y. Song, M. M. Doeff and T. J. Richardson, *Energy Environ. Sci.*, 2011, **4**, 885.
8 Z. Xing, Z. C. Ju, J. Yang, H. Y. Xu and Y. T. Qian, *Nano Res.*, 2012, **5**, 477.
9 P. Poizot, S. Laruelle, S. Grugeon, L. Dupont and J. M. Tarascon, *Nature*, 2000, **407**, 496.
10 F. M. Zhan, B. Y. Geng and Y. J. Guo, *Chem.–Eur. J.*, 2009, **15**, 6169.
11 X. Wang, X. L. Wu, Y. G. Guo, Y. T. Zhong, X. Q. Cao, Y. Ma and J. N. Yao, *Adv. Funct. Mater.*, 2010, **20**, 1680.
12 K. T. Nam, D. W. Kim, P. J. Yoo, C. Y. Ching, N. Meethong, P. T. Hammond, Y. M. Chiang and A. M. Belcher, *Science*, 2006, **312**, 885.
13 M. H. Park, M. G. Kim, J. Joo, K. Kim, J. Ki, S. Ahn, Y. Cui and J. Cho, *Nano Lett.*, 2009, **9**, 3844.
14 C. K. Chan, H. Peng, G. Liu, K. McIlwrath, X. F. Zhang, R. A. Huggins and Y. Cui, *Nat. Nanotechnol.*, 2008, **3**, 31.
15 A. Madasinski, P. Dixon, B. Hertzberg, A. Kvit, J. Ayala and G. Yushin, *Nat. Mater.*, 2010, **9**, 353.
16 G. Amatucci and J. M. Tarascon, *J. Electrochem. Soc.*, 2002, **149**, K31.
17 Y. G. Wang, H. Q. Li, P. He, E. Hosono and H. S. Zhou, *Nanoscale*, 2010, **2**, 1294.
18 H. W. Lee, P. Muralidharan, R. Ruffo, C. M. Mari, Y. Cui and D. K. Kim, *Nano Lett.*, 2010, **10**, 3852.
19 A. Vu, Y. Q. Qian and A. Stein, *Adv. Energy Mater.*, 2012, **2**, 1056.
20 Z. J. Han, N. Yabuuchi, K. Shimomura, M. Murase, H. Yui and S. Komaba, *Energy Environ. Sci.*, 2012, **5**, 9014.
21 F. Y Cheng, H. B. Wang, Z. Q. Zhu, Y. Wang, T. R. Zhang, Z. L. Tao and J. Chen, *Energy Environ. Sci.*, 2011, **4**, 3668.
22 D. M. Yu, C. G. Chen, S. H. Xie, Y. Y. Liu, K. Park, X. Y. Zhou, Q. F. Zhang, J. Y. Lic and G. Z. Cao, *Energy Environ. Sci.*, 2011, **4**, 858.
23 Y. Deng, S. D. Tang, Q. M. Zhang, Z. Shi, L. Zhang, S. Zhan and G. H. Chen, *J. Mater. Chem.*, 2011, **21**, 11987.
24 Y. Yang, Y. Q. Zhao, L. F. Xiao and L. Z. Zhang, *Electrochem. Commun.*, 2008, **10**, 1117.
25 S. W. Kim, H. W. Lee, P. Muralidharan, D. H. Seo, W. S. Yoon, D. K. Kim and K. Kang, *Nano Res.*, 2011, **4**, 505.
26 F. M. Courtel, H. Duncan, Y. Abu-Lebdeh and I. J. Davidson, *J. Mater. Chem.*, 2011, **21**, 10206.
27 G. Q. Zhang, L. Yu, W. B. Hao and X. W. Lou, *Adv. Mater.*, 2012, **24**, 4609.
28 L. F. Xiao, Y. Y. Yang, J. Yin, Q. Li and L. Z. Zhang, *J. Power Sources*, 2009, **194**, 1089.
29 J. Zhao, F. Q. Wang, P. P. Su, M. R. Li, J. Chen, Q. H. Yang and C. Li, *J. Mater. Chem.*, 2012, **22**, 13328.
30 Z. C. Bai, B. Sun, N. Fan, Z. C. Ju, M. H. Li, L. Q. Xu and Y. T. Qian, *Chem.–Eur. J.*, 2012, **18**, 5319.
31 Z. C. Bai, N. Fan, Z. C. Ju, C. H. Sun and Y. T. Qian, *Mater. Lett.*, 2012, **76**, 124.
32 L. W. Zhang, H. Y. Cheng, R. L. Zong and Y. F. Zhu, *J. Phys. Chem. C*, 2009, **113**, 2368.
33 P. K. Sharma and M. S. Whittingham, *Mater. Lett.*, 2001, **48**, 319.
34 F. Jiao, J. Bao, A. H. Hill and P. G. Bruce, *Angew. Chem., Int. Ed.*, 2008, **47**, 9711.

35 J. Guan and M. Liu, *Solid State Ionics*, 1998, **110**, 21.
36 Y. G. Zhang, Y. Liu, F. Guo, Y. H. Hu, X. Z. Liu and Y. T. Qian, *Solid State Commun.*, 2005, **134**, 523.
37 X. W. Lou, L. A. Archer and Z. C. Yang, *Adv. Mater.*, 2008, **20**, 3987.
38 Y. Cao, L. Xiao, X. Ai and H. Yang, *Electrochem. Solid-State Lett.*, 2003, **6**, A30.
39 H. Li, X. Huang and L. Chen, *Solid State Ionics*, 1999, **123**, 189.
40 G. Binotto, D. Larcher, A. S. Prakash, R. H. Urbina, M. S. Hegde and J. M. Tarascon, *Chem. Mater.*, 2007, **19**, 3032.
41 F. M. Courtel, Y. Abu-Lebdeh and I. J. Davidson, *Electrochim. Acta*, 2012, **71**, 123.